Open Access Research Journal of
Chemistry and Pharmacy
Journals home page: https://oarjpublication/journals/oarjcp/
ISSN: 2783-0276 (Online)

OARJ OPEN ACCESS RESEARCH JOURNALS

(RESEARCH ARTICLE)

Check for updates

Synthesis, spectral characterization, magnetic, thermal and molecular docking studies of new thiosemicarbazone-based Schiff base ligands derived from Benzil and Benzoin, and Their Co (II) and Ni (II) Complexes

Nabaa N. Mohammed [1,*], Wurood A. Jaafar [2] and Noha Ali Hadi [3]

[1] *Department of Chemistry, College of Education for Pure Sciences, University of Samarra, Samarra, Iraq.*
[2] *Department of Chemistry, College of Applied Sciences, University of Samarra, Samarra, Iraq.*
[3] *Department of Chemistry, College of Education for Pure Sciences (Ibn Al-Haitham), University of Baghdad, Baghdad, Iraq.*

Open Access Research Journal of Chemistry and Pharmacy, 2026, 09(01), 028–054

Publication history: Received on 29 June 2026; revised on 06 August 2026; accepted on 08 August 2026

Article DOI: https://doi.org/10.53022/oarjcp.2026.9.1.0024

Abstract

Two new thiosemicarbazone-type Schiff base ligands, [L1] and [L2], were synthesized in high purity by refluxing (7 h, 70–75 °C, glacial acetic acid catalyst) an ethanolic solution of N-phenylhydrazinecarbothioamide with benzil and benzoin, respectively, and were subsequently reacted with hydrated CoCl2 and NiCl2 (2:1 ligand:metal molar ratio, 4 h reflux at 70–75 °C) to give the corresponding octahedral Co(II) and Ni(II) chelates. The ligands and their metal complexes were characterized by melting point, yield, elemental composition, FT-IR, UV-Visible, 1H- and 13C-NMR, mass spectrometry, magnetic susceptibility, thermogravimetric analysis (TGA), and frontier molecular orbital (HOMO/LUMO) calculations. The spectral evidence supports coordination of the metal ions through the azomethine nitrogen and thioamide sulfur/nitrogen donor sites, giving predominantly octahedral geometries for the hydrated Co(II) and Ni(II) chelates, in agreement with their measured magnetic moments. Molecular docking of L1 and L2 against the human enzyme Phosphodiesterase 3A (PDE3A) was performed to evaluate their potential as enzyme-binding scaffolds, and the resulting binding energies, hydrogen-bonding interactions and docking scores are reported and discussed in the context of the reported pharmacological relevance of PDE3A.

Keywords: Schiff Base; Thiosemicarbazone; Co(II)/Ni(II) Complexes; Magnetic Moment; TGA; Molecular Docking; Phosphodiesterase 3A (PDE3A)

1. Introduction

Schiff bases, formed by the condensation of a primary amine with an active carbonyl compound to give an azomethine (–C=N–) linkage, remain among the most widely studied classes of ligands in coordination chemistry because of the ease of their synthesis, the structural versatility of the imine donor group, and the diverse geometries they can impose on the metal ions they chelate [1].

Thiosemicarbazones, obtained by condensing thiosemicarbazide derivatives with aldehydes or ketones, constitute an important subclass of Schiff bases. Their soft sulfur and hard nitrogen donor atoms make them efficient bidentate or tridentate NS/NNS chelating agents capable of stabilizing a wide range of transition-metal oxidation states, and their multidonor character underlies much of the pronounced biological activity reported for their metal chelates [2,3].

Beyond their coordination behavior, Schiff bases and their transition-metal complexes have attracted continuous attention for their antimicrobial, antioxidant, antiviral and anticancer properties, which has encouraged the combined use of spectroscopic, magnetic, thermal and computational (DFT and molecular docking) tools to rationalize structure-activity relationships in this class of compounds [4,5].

* Corresponding author: Nabaa N. Mohammed

Cyclic-nucleotide phosphodiesterase 3A (PDE3A), which hydrolyzes cAMP and cGMP and thereby regulates intracellular second-messenger signaling, has been implicated in cardiovascular, inflammatory and oncological processes, and is currently explored both as a drug target and, through its non-catalytic partnership with SLFN12, as a determinant of selective cancer-cell cytotoxicity [6,7].

Because coordination of azomethine and thioamide donor ligands to a metal center can modulate lipophilicity, electronic distribution and hydrogen-bonding capacity, in silico docking against pharmacologically relevant protein targets such as PDE3A provides a useful preliminary screen for the biological potential of newly synthesized Schiff base ligands, complementing their conventional physicochemical characterization [8].

In the present work, two Schiff base ligands, L1 (derived from benzil) and L2 (derived from benzoin), each bearing the N-phenylhydrazinecarbothioamide (thiosemicarbazide) framework, were prepared and fully characterized, and their Co(II) and Ni(II) chelates were synthesized and studied by a combination of spectroscopic, magnetic, thermal and computational methods, culminating in a molecular docking evaluation against PDE3A.

2. Experimental

2.1. Materials and physical measurements

Benzil, benzoin, N-phenylhydrazinecarbothioamide, absolute ethanol, glacial acetic acid, and hydrated CoCl2 and NiCl2 were used as received without further purification. Melting points were determined and are uncorrected. FT-IR spectra were recorded as KBr discs, UV-Visible spectra in suitable solvents, and 1H- and 13C-NMR spectra in deuterated solvents; mass spectra were obtained by electron-impact/ESI ionization. Magnetic susceptibilities of the solid complexes were measured at room temperature and corrected for diamagnetism; thermogravimetric analysis (TGA) was carried out under an inert atmosphere from room temperature to above 600 °C.

2.2. Synthesis of the Schiff base ligand [L1]

Benzil (2 g, 9.43 mmol) was dissolved in absolute ethanol (40 mL) in a 250 mL round-bottom flask immersed in a water bath, and a few drops of glacial acetic acid were added as catalyst; the mixture was stirred and gently heated for about 10 min. In a separate 100 mL beaker, N-phenylhydrazinecarbothioamide (1.59 g, 9.57 mmol) was dissolved in absolute ethanol (40 mL) to give a clear solution, which was then added gradually to the benzil solution with continuous stirring to give a yellow solution. The mixture was refluxed for 7 h at 70–75 °C and then allowed to cool, depositing a pale-yellow precipitate. The product was filtered off, washed with cold ethanol, and dried to give [L1] as pale-yellow needle-like crystals (2 g, 58%), m.p. 158–160 °C.

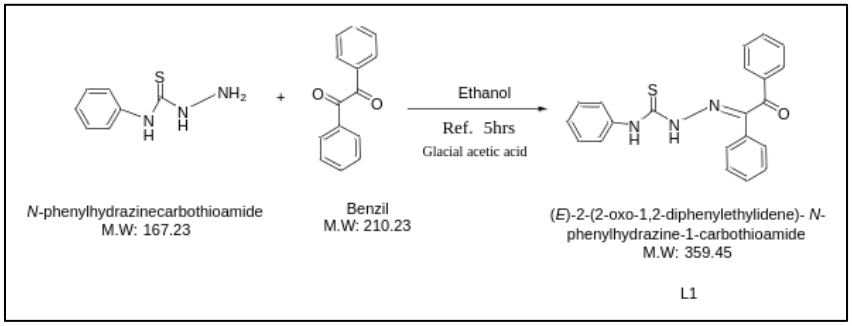

Scheme 1 Synthetic route to the Schiff base ligand [L1]

2.3. Synthesis of the Co(II) and Ni(II) complexes of [L1]

In a 250 mL round-bottom flask, [L1] (0.5 g, 1.01 mmol) was dissolved in absolute ethanol (20 mL) with mild heating. A solution of CoCl2·6H2O (0.165 g, 0.5 mmol) in ethanol (5 mL) was added gradually with continuous stirring in a 2:1 (ligand:metal) molar ratio. The mixture was refluxed for 4 h at 70–75 °C, depositing a colored microcrystalline precipitate, which was filtered off, washed with cold ethanol, and dried to give [Co(L1)2] in 50% yield (m.p. 78–80 °C). The Ni(II) complex, [Ni(L1)2], was prepared analogously using NiCl2·6H2O in place of CoCl2·6H2O. Table 1 summarizes the amounts of metal salt and ligand used, together with the proposed empirical formulae, colors, melting points and yields of the [L1] complexes.

Table 1 Preparation data and physical properties of the [L1] complexes

No.	Metal salt	Weight of ligand (g)	Weight of metal salt (g)	Empirical formula	Color	M.P (°C)	Yield (%)
1	CoCl2·6H2O	0.5	0.165	[Co(C42H34N6O2S2)]	Black	78–80	50
2	NiCl2·6H2O	0.5	0.36	[Ni(C42H34N6O2S2)]	Reddish brown	205–208	100

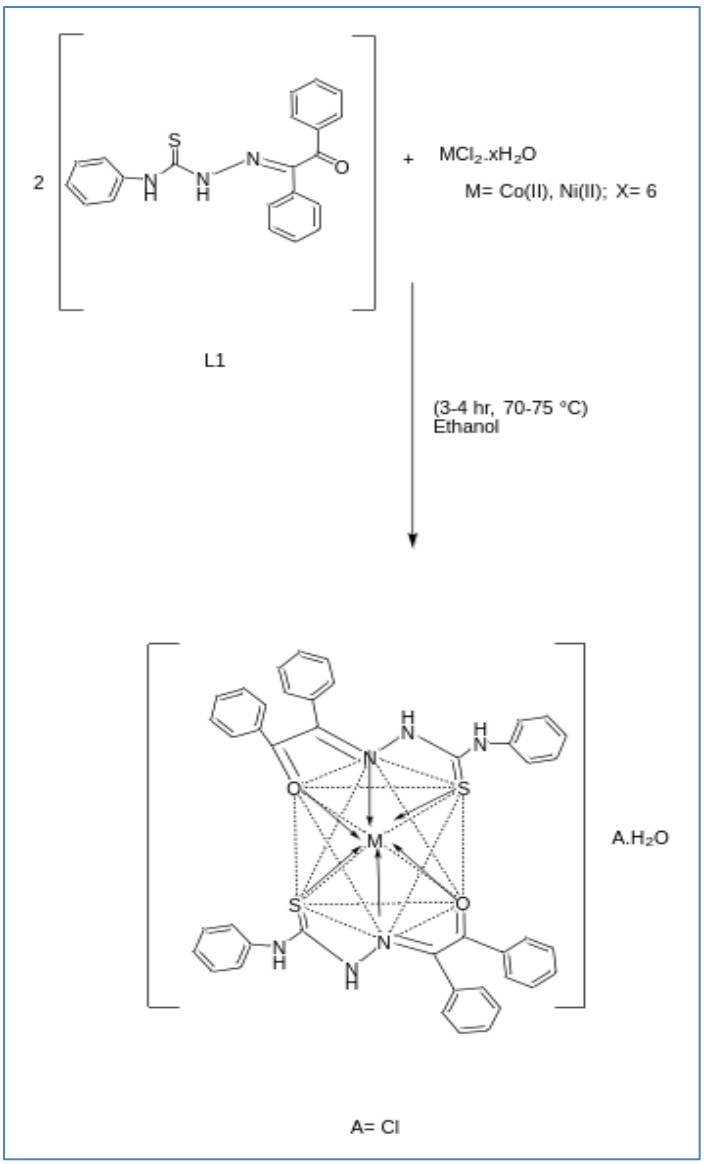

Scheme 2 Synthetic route to the Co(II) and Ni(II) complexes of [L1]

2.4. Synthesis of the Schiff base ligand [L2]

Benzoin (2 g, 9.43 mmol) was dissolved in absolute ethanol (40 mL) in a 250 mL round-bottom flask immersed in a water bath, and a few drops of glacial acetic acid were added; the mixture was stirred and gently heated for about 10 min. N-Phenylhydrazinecarbothioamide (1.57 g, 9.57 mmol) was dissolved separately in absolute ethanol (40 mL) to give a clear solution, which was added gradually to the benzoin solution with continuous stirring to give a yellow solution. The mixture was refluxed for 7 h at 70–75 °C and then allowed to cool, depositing a greenish-yellow precipitate. The product was filtered off, washed with cold ethanol, and dried to give [L2] as transparent, pale-yellow cylindrical crystals (1.5 g, 44%), m.p. 112–115 °C.

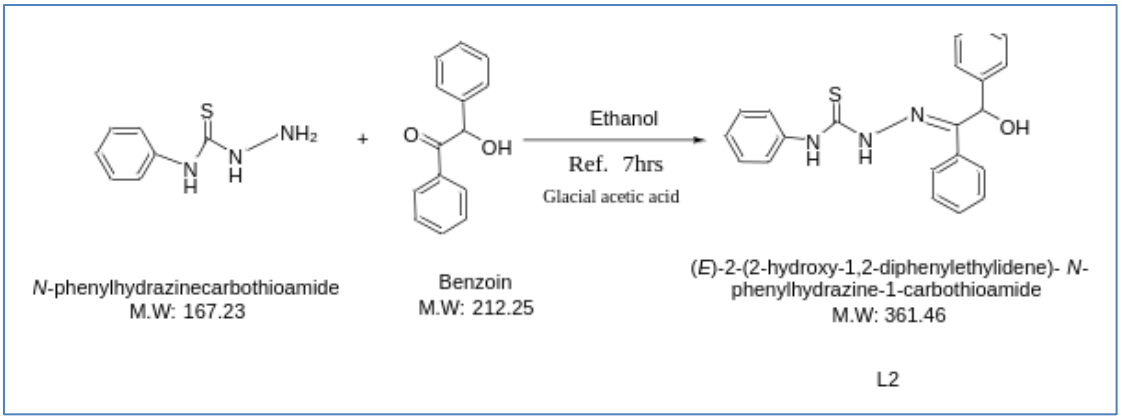

Scheme 3 Synthetic route to the Schiff base ligand [L2]

2.5. Synthesis of the Co(II) and Ni(II) complexes of [L2]

In a 250 mL round-bottom flask, [L2] (0.36 g, 1.01 mmol) was dissolved in absolute ethanol (20 mL) with mild heating. A solution of CoCl2·6H2O (0.084 g, 0.5 mmol) in ethanol (5 mL) was added gradually with continuous stirring in a 2:1 (ligand:metal) molar ratio. The mixture was refluxed for 4 h at 70–75 °C, depositing a colored precipitate, which was filtered off, washed with cold ethanol, and dried to give [Co(L2)2]·H2O in 75% yield, m.p. 120–125 °C. The Ni(II) complex, [Ni(L2)2], was prepared analogously using NiCl2·6H2O in place of CoCl2·6H2O. Table 2 summarizes the corresponding preparation data for the [L2] complexes.

Table 2 Preparation data and physical properties of the [L2] complexes

No.	Metal salt	Weight of ligand (g)	Weight of metal salt (g)	Empirical formula	Color	M.P (°C)	Yield (%)
1	CoCl2·6H2O	0.25	0.084	[Co(C42H38N6O2S2)]	Reddish brown	120–125	75
2	NiCl2·6H2O	1	0.33	[Ni(C42H38N6O2S2)]	Light purple	–	68

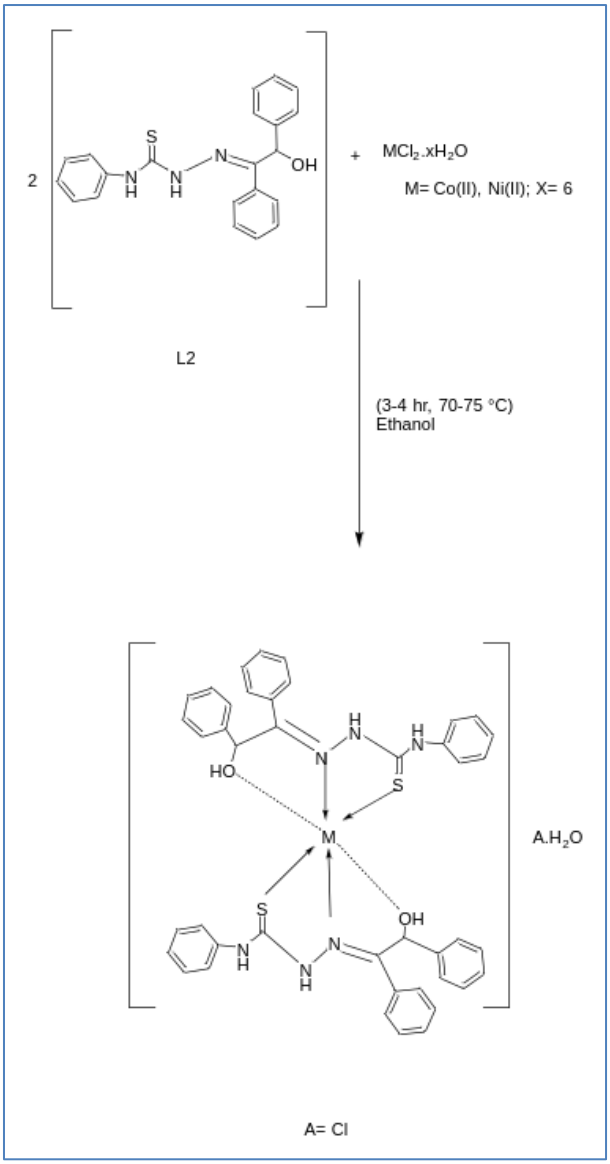

Scheme 4 Synthetic route to the Co(II) and Ni(II) complexes of [L2]

3. Results and Discussion

3.1. Physical and analytical data

The two Schiff base ligands were obtained as air-stable, colored crystalline solids in moderate-to-good yield, with sharp melting points confirming their purity (Table 3); the higher melting point of [L1] relative to [L2] is consistent with the more rigid, fully conjugated benzil-derived backbone of the former, and both isolated yields (58% for [L1], 44% for [L2]) and melting points agree closely with the values recorded during synthesis (Sections 2.2 and 2.4) [9].

Table 3 Physical and analytical characteristics of the Schiff base ligands

Compound	Molecular formula	M.wt (g/mol)	M.P (°C)	Color	Yield (%)
Ligand [L1]	C21H17N3OS	359.4	158–160	Yellow	58
Ligand [L2]	C21H19N3OS	361.4	112–115	Orange	44

3.2. Infrared (FT-IR) spectra

Comparison of the IR spectra of the free starting materials (benzil, N-phenylhydrazinecarbothioamide, benzoin) with those of the Schiff base ligands provided direct evidence for imine (Schiff base) formation and for the coordination environment offered to a metal ion, since condensation of the carbonyl/hydrazide precursors is expected to remove the free NH2 and ketonic C=O stretching bands while generating a new, diagnostic azomethine (C=N) absorption [2,10].

In [L1], the disappearance of the free ν(NH2) band of N-phenylhydrazinecarbothioamide, together with the persistence of a ν(NH) band near 3178 cm^{-1} and a band at 1662 cm^{-1} assigned jointly to ν(C=N) imine and thioamide ν(C=S), is consistent with cyclization/thioamide tautomerism accompanying Schiff base formation from the diketone benzil; the aromatic ν(C=C) bands at 1593 and 1500 cm^{-1} and the aliphatic/aromatic ν(C-H) bands near 2978 and 3101–3063 cm^{-1} confirm retention of the phenyl rings[1,11] .

In [L2], retention of a broad band at 3298 cm^{-1} (overlapping ν(NH)/ν(OH) of the residual benzoin hydroxyl) together with the new ν(C=N) band at 1658 cm^{-1} and the ν(C-N)/ν(N-N) bands in the 1315–1177 cm^{-1} region support formation of the hydrazono-thioamide linkage while a free secondary alcohol group is retained, consistent with the asymmetric benzoin-derived structure of this ligand [10].

Table 4 Principal IR absorption bands (cm^{-1}) of the starting materials and the ligands [L1] and [L2]

Compound	**ν(NH2)**	**ν(NH)**	**ν(C=C) arom.**	**ν(C=N) imine**	**ν(C=O)**	**ν(OH)**	**ν(C-N)/(N-N)**	**ν(C-H) arom.**	**ν(C-H) aliph.**	**ν(C=S)**
Benzil	-	-	1616, 1593	-	1654–1616	-	-	3063	-	-
N-Phenylhydrazinecarbothioamide	3302, 3155	3302, 3155	1593, 1523	-	-	-	1281–1022	3101–3063	2970	1280-690
[L1]	-	3178	1593, 1504	1662 (m)	1662	-	1315–1010	3101–3063	2978	1265-690
Benzoin	-	-	1600–1450	-	1678	3400–3200 (s)	-	3100–3030	2980–2850	-
[L2]	-	3198–3175	1593, 1543,1489	1681	-	3197	1315–1176	3101, 3067	2978	1261–690

Sh = Sharp, W = Weak, S = Strong, m = medium

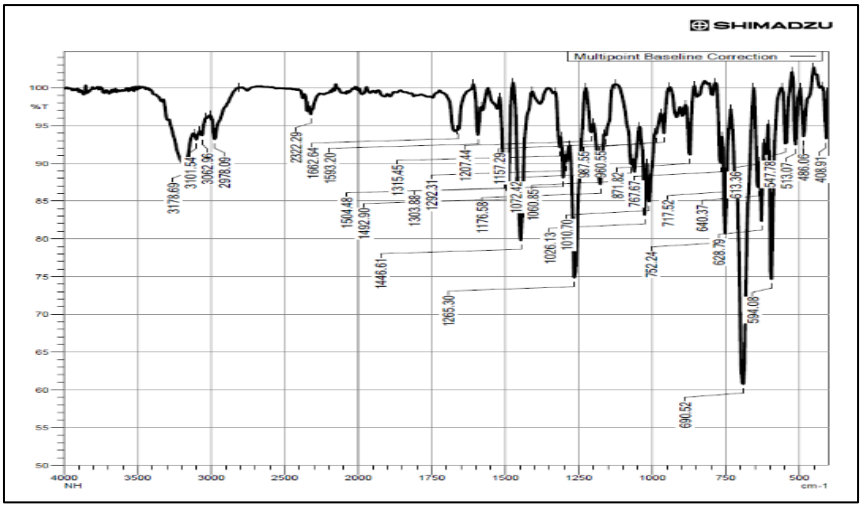

Figure 1 FT-IR spectrum of the Schiff base ligand [L1]

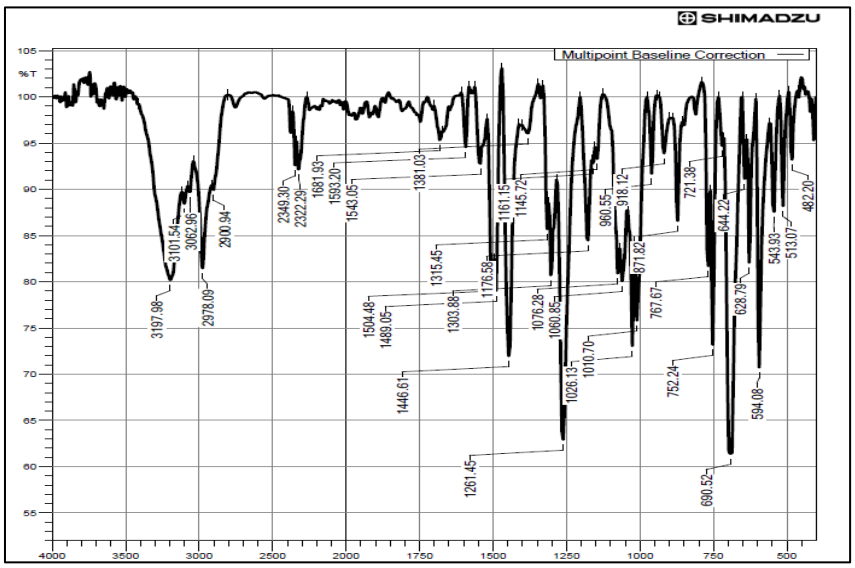

Figure 2 FT-IR spectrum of the Schiff base ligand [L2]

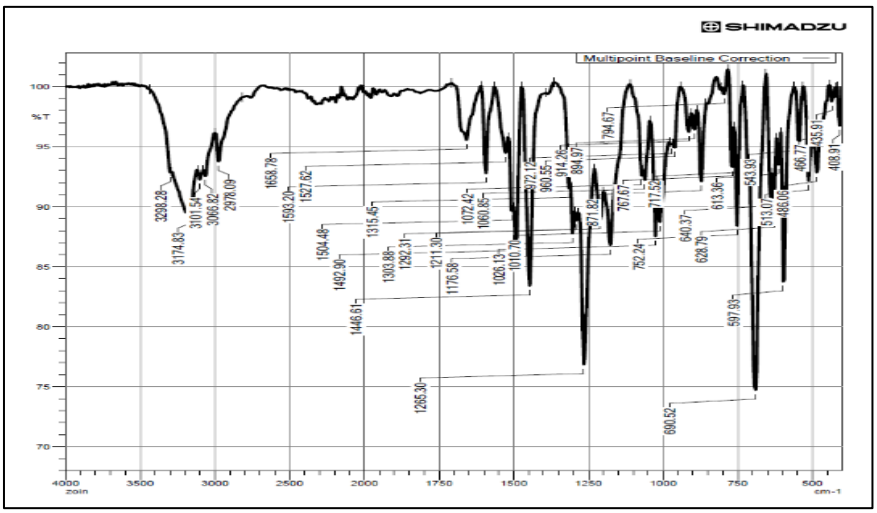

Figure 3 FT-IR spectrum of the complex [Co(L1)2]·H2O

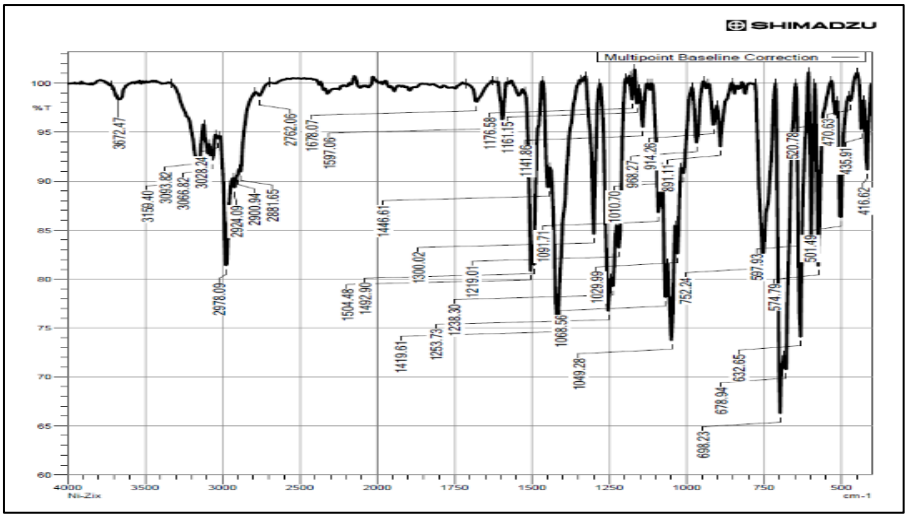

Figure 4 FT-IR spectrum of the complex [Ni(L1)2]·H2O

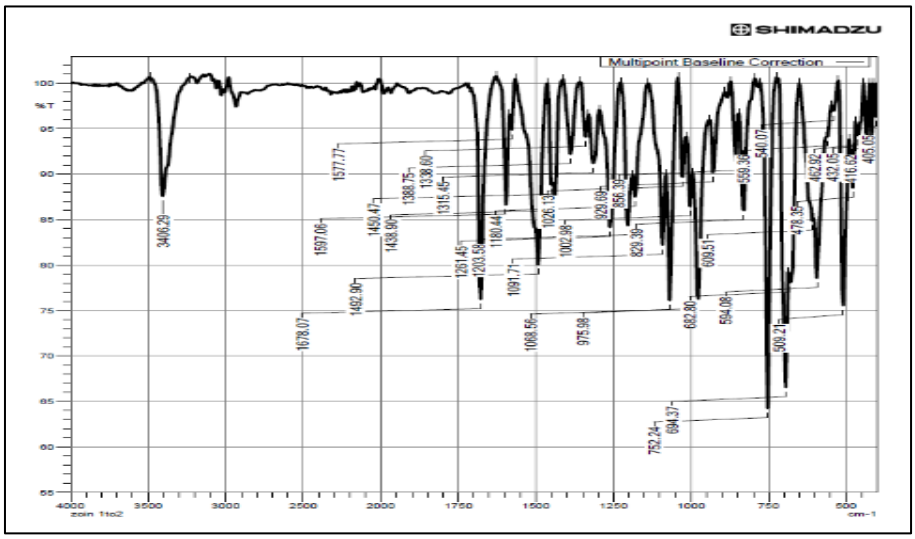

Figure 5 FT-IR spectrum of the complex [Co(L2)2]·H2O

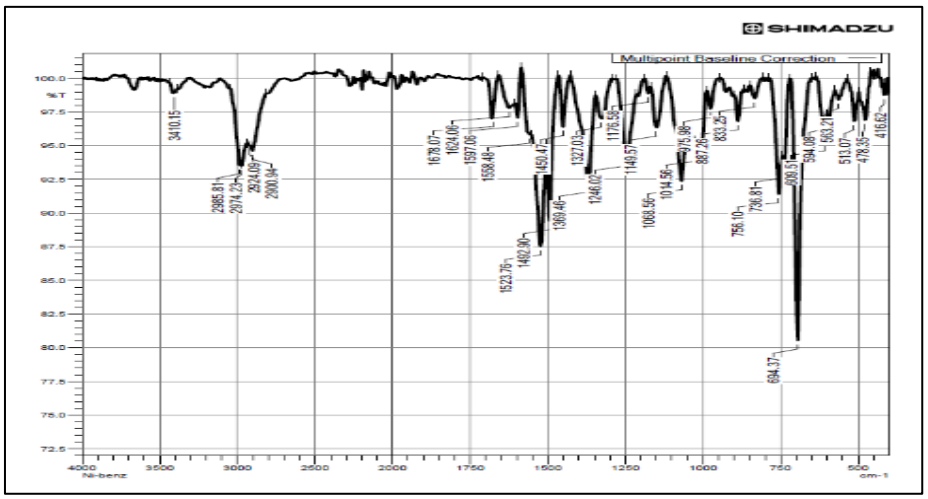

Figure 6 FT-IR spectrum of the complex [Ni(L2)2]·H2O

3.3. Electronic (UV-Visible) spectra

The electronic absorption spectra of the free ligands [L1] and [L2] each display three characteristic intraligand transitions: a high-energy π→π* band near 202–204 nm arising from the aromatic and azomethine chromophores, a second π→π* band, and a lower-energy n→π* band in the 250–330 nm region attributable to the lone pairs on the imine nitrogen and thioamide sulfur atoms, in line with the assignment pattern generally reported for thiosemicarbazone-derived Schiff bases[12, 13].

Table 5 Electronic (UV-Vis) spectral data of the ligands [L1] and [L2]

Compound	Transition	λ (nm)	υ (cm^{-1})	εmax ($L \cdot mol^{-1} \cdot cm^{-1}$)
[L1]	π→π*	202.5	49383	880
	π→π*	250	38462	330
	n→π*	330	31250	230
[L2]	π→π*	204	49020	1600
	π→π*	250	40000	850
	n→π*	320	31250	200

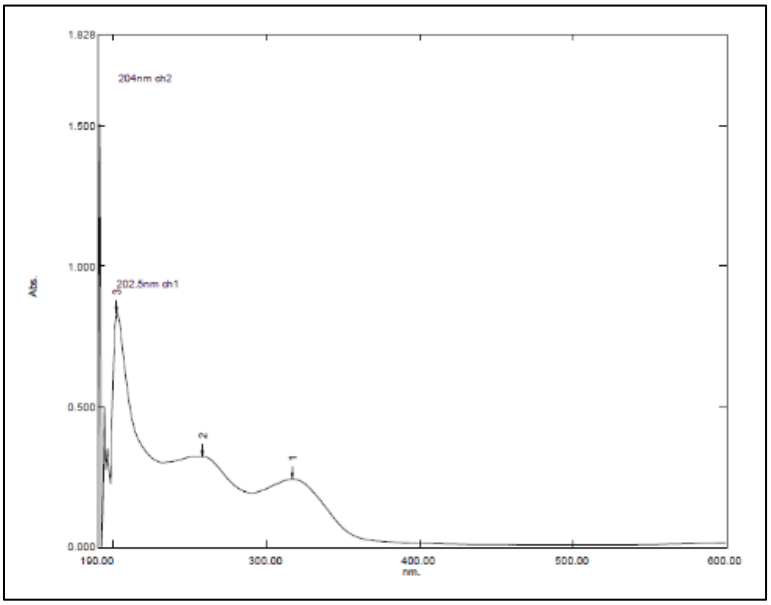

Figure 7 UV-Visible spectrum of the Schiff base ligand [L1]

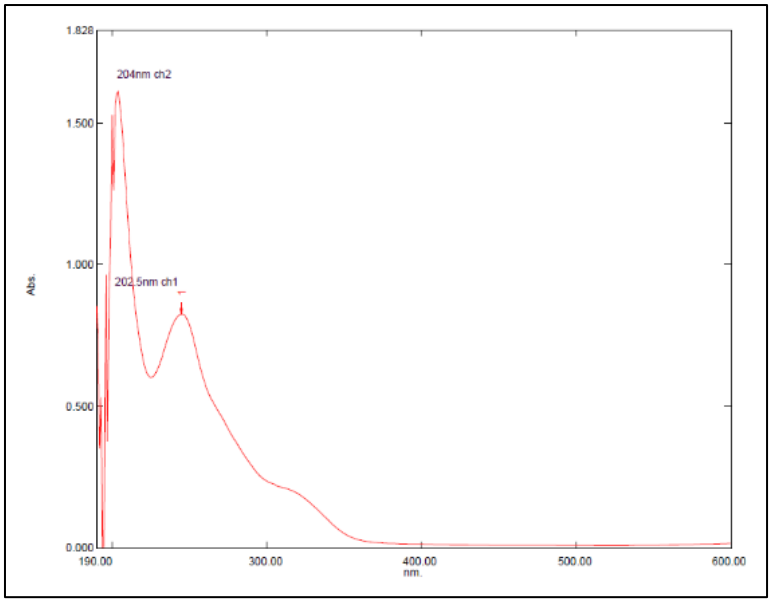

Figure 8 UV-Visible spectrum of the Schiff base ligand [L2]

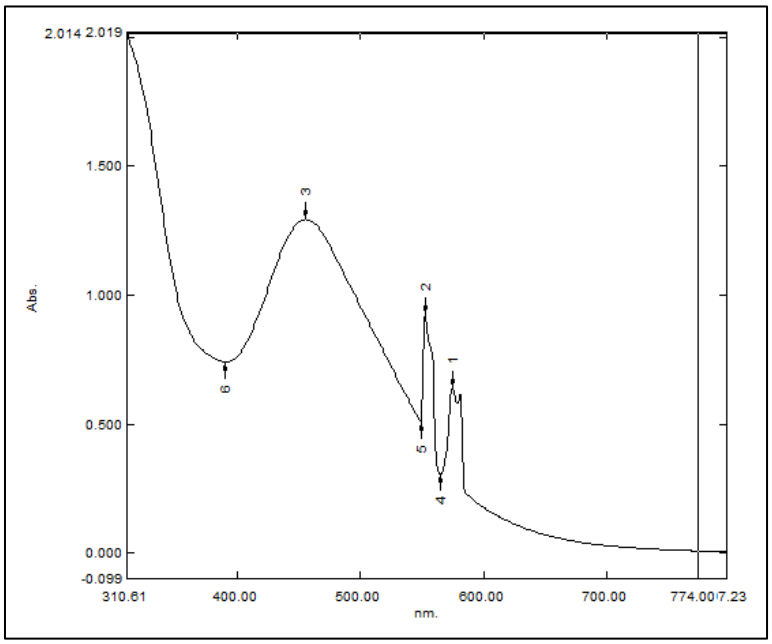

Figure 9 UV-Visible spectrum of the complex [Co(L1)2]

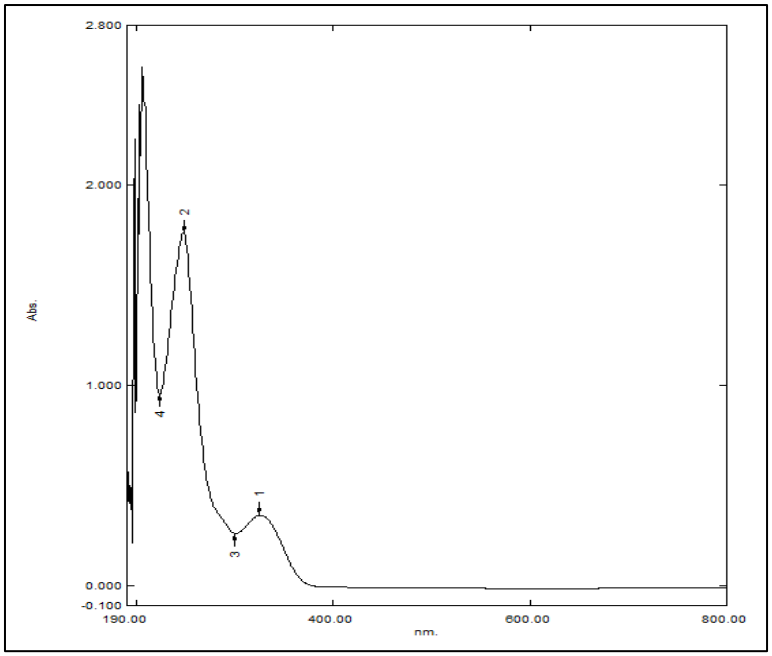

Figure 10 UV-Visible spectrum of the complex [Ni(L1)2]

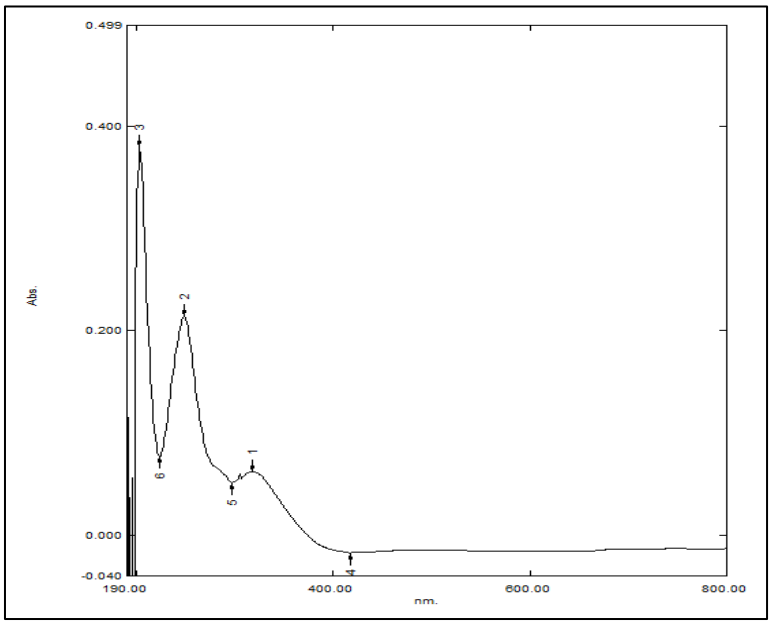

Figure 11 UV-Visible spectrum of the complex [Co(L2)2]

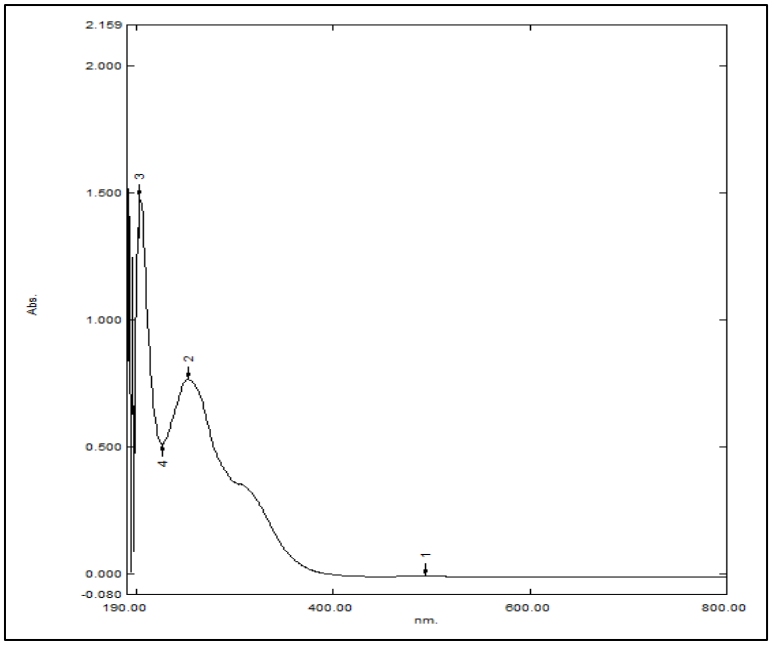

Figure 12 UV-Visible spectrum of the complex [Ni(L2)2]

Upon complexation, the electronic spectra of the [L1]- and [L2]-based Co(II) and Ni(II) chelates (recorded in ethanol at 10^{-3} M) show, in addition to the retained intraligand π→π*/n→π* bands, new low-energy visible bands assigned to ligand-to-metal charge-transfer (LMCT) transitions overlapping spin-allowed d-d transitions, which is diagnostic of coordination through the azomethine nitrogen and thioamide donor atoms [11,13].

Table 6 Electronic spectral data of the [L1] complexes (10^{-3} M in ethanol)

Compound	λ (nm)	ῡ (cm^{-1})	Abs.	Transition	Proposed geometry
[L1]	340	29412	19	n→π*	–
	201	49751	586	π→π*	
[Co(L1)2]·H2O	456	21930	1.293	LMCT + d-d	Octahedral
	260	38462	0.232	π→π*, n→π*	
	202	49505	0.400	π→π*	
[Ni(L1)2]·H2O	494	20243	0.474	LMCT, d-d	Octahedral
	325	30769	0.135	n→π*	
	248	40323	0.303	π→π*	

For the [Co(L1)2]·H2O complex, the visible band at 456 nm is consistent with an octahedral Co(II) chromophore, while for [Ni(L1)2]·H2O the corresponding band at 494 nm is likewise consistent with an octahedral Ni(II) environment, in agreement with the six-coordinate geometry proposed from the magnetic and IR data (Section 3.6) [10,14].

Table 7 Electronic spectral data of the [L2] complexes (10^{-3} M in ethanol)

Compound	λ (nm)	ῡ (cm^{-1})	Abs.	Transition	Proposed geometry
[L2]	363.20	27536	1177	n→π*	–
	277.20	36071	235	π→π*	
	255.00	39216	845	π→π*	
[Co(L2)2]·H2O	582	17182	0.383	^{4}T1g(F)→^{4}A2g(F)	Octahedral

	553	18083	0.523	^{4}T1g(F)→^{4}T1g(P)	
	317	31546	0.062	Charge transfer	
	248	40323	0.214	π→π*	
	203	49261	0.380	n→π*	
[Ni(L2)2]·H2O	494	20243	0.474	^{3}A2g(F)→^{3}T1g(d-d)	Octahedral
	252	39683	0.766	π→π*	
	203	49261	1.483	π→π*	

The [Co(L2)2]·H2O spectrum shows the two spin-allowed bands ^{4}T1g(F)→^{4}A2g(F) and ^{4}T1g(F)→^{4}T1g(P), which are characteristic of high-spin octahedral Co(II), while the [Ni(L2)2]·H2O spectrum shows the ^{3}A2g(F)→^{3}T1g(d-d) transition characteristic of octahedral Ni(II); together with the corresponding data for the [L1] complexes, these assignments provide direct electronic-spectral evidence that all four chelates adopt six-coordinate octahedral geometries around the metal center, most likely completed by coordinated/lattice water molecules and consistent with the general formula [M(L)2]·H2O [10,15].

3.4. 1H- and 13C-NMR spectra

The 1H- and 13C-NMR spectra of [L1] and [L2] were recorded in deuterated DMSO-d6, and the observed chemical shifts were assigned by comparison with the expected proton- and carbon-bearing environments of the proposed structures, providing further confirmation of Schiff base formation and, for [L1], of the retained free ketone carbonyl [9,16].

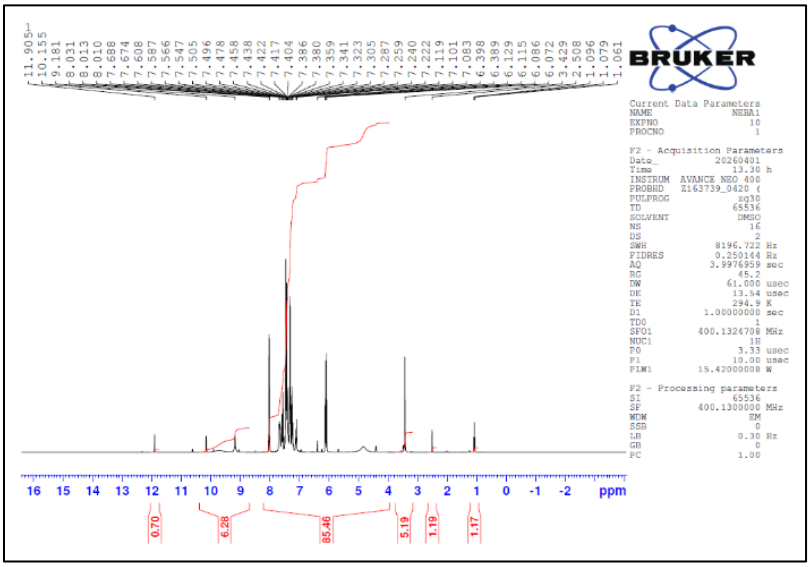

Figure 13 1H-NMR spectrum of the Schiff base ligand [L1]

The 1H-NMR spectrum of [L1] (DMSO-d6, residual solvent signal at δH = 2.5 ppm) showed a singlet at δH = 11.90 ppm assigned to the thioamide (NH–C=S) proton, a singlet at δH = 10.15 ppm assigned to the NH proton adjacent to the phenyl-substituted nitrogen, a further singlet at δH = 9.18 ppm assigned to the proton associated with the hydrazone (C=N–NH) linkage, and a multiplet in the δH = 7.08–8.03 ppm region assigned to the aromatic protons of the three phenyl rings [9].

Table 8 1H-NMR spectral data of the Schiff base ligands [L1] and [L2] (DMSO-d6)

Compound	δH (ppm)	Multiplicity	Assignment
[L1]	11.90	s	NH–C=S (thioamide NH)
	10.15	s	NH adjacent to the N-phenyl group

	9.18	s	NH of the hydrazone (C=N–NH) linkage
	7.08–8.03	m	Aromatic protons of the three phenyl rings
[L2]	12.29	s	NH attached to the thioamide (C=S) group
	8.47	s	NH adjacent to the azomethine (C=N) bond
	7.95, 6.90	s/m	Aromatic ring protons
	6.13	s	CH proton adjacent to the OH group
	3.37–3.40	s	OH proton

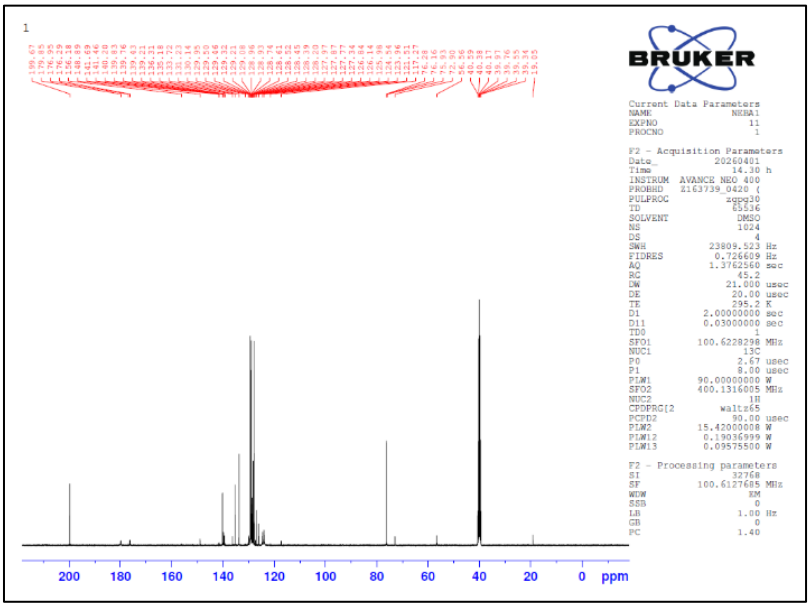

Figure 14 13C-NMR spectrum of the Schiff base ligand [L1]

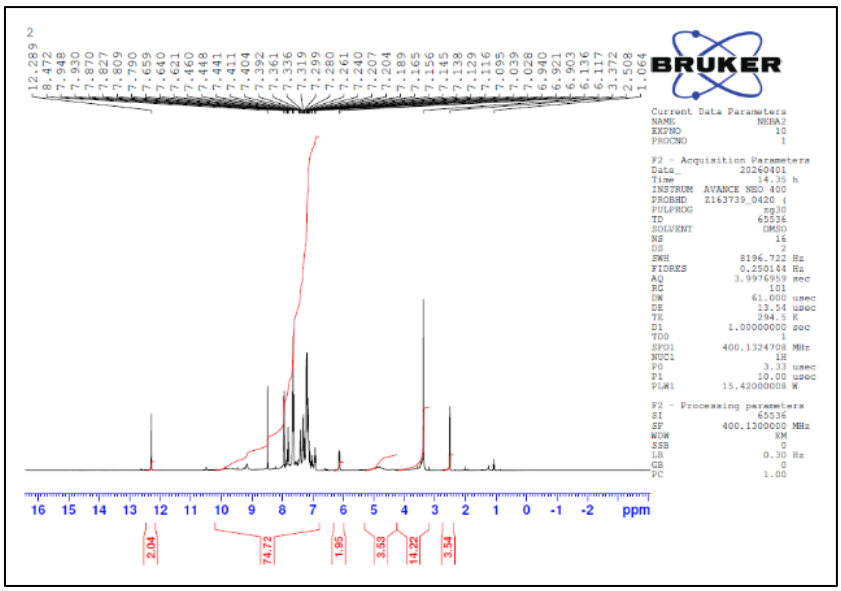

Figure 15 1H-NMR spectrum of the Schiff base ligand [L2]

The 13C-NMR spectrum of [L1] (DMSO-d6) showed a signal at δC = 199.67 ppm assigned to the retained, unreacted ketone (C=O) carbon, a signal at δC = 179.85–176.29 ppm assigned to the thiocarbonyl (C=S) carbon, a signal at δC = 156.18 ppm assigned to the azomethine (C=N) carbon, signals at δC = 148–136 ppm assigned to the aromatic (ipso)

carbon adjacent to the imine group, further aromatic carbons at δC = 133–124 ppm and δC = 121.51–117.27 ppm, and a signal at δC = 39.34 ppm overlapping with the DMSO-d6 solvent carbon signal [16].

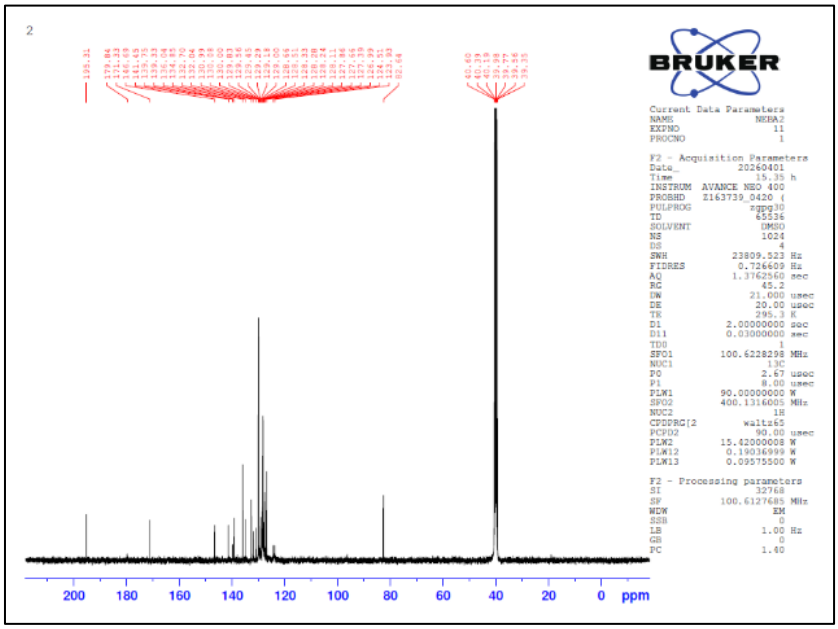

Figure 16 13C-NMR spectrum of the Schiff base ligand [L2]

The 13C-NMR spectrum of [L2] (DMSO-d6) showed a signal at δC = 179.84 ppm assigned to the thiocarbonyl (C=S) carbon, a signal at δC = 146.69 ppm assigned to the azomethine (C=N) carbon, aromatic ipso-carbon signals at δC = 141.45, 139.75, 139.33 and 136.04 ppm directly attached to the two phenyl rings and the conjugated hydrazone system, further aromatic carbons at δC = 134.85, 127–131 and 123.93 ppm, a signal at δC = 82.64 ppm assigned to the methine (CH–OH) carbon, and signals at δC = 39.35–40.60 ppm attributed to the DMSO-d6 solvent [9].

Table 9 13C-NMR spectral data of the Schiff base ligands [L1] and [L2] (DMSO-d6)

Compound	δC (ppm)	Assignment
[L1]	199.67	Retained ketone (C=O) carbon
	179.85–176.29	Thiocarbonyl (C=S) carbon
	156.18	Azomethine (C=N) carbon
	148–136	Aromatic ipso-carbon adjacent to the imine group
	133–124 / 121.51–117.27	Aromatic ring carbons
	39.34*	Overlapping with DMSO-d6 solvent signal
[L2]	179.84	Thiocarbonyl (C=S) carbon
	146.69	Azomethine (C=N) carbon
	141.45, 139.75, 139.33, 136.04	Aromatic ipso-carbons attached to the phenyl rings/conjugated system
	134.85, 127–131, 123.93	Aromatic ring carbons
	82.64	Methine (CH–OH) carbon
	39.35–40.60*	DMSO-d6 solvent carbons

*Solvent (DMSO-d6) signal region.

3.5. Mass spectrometry

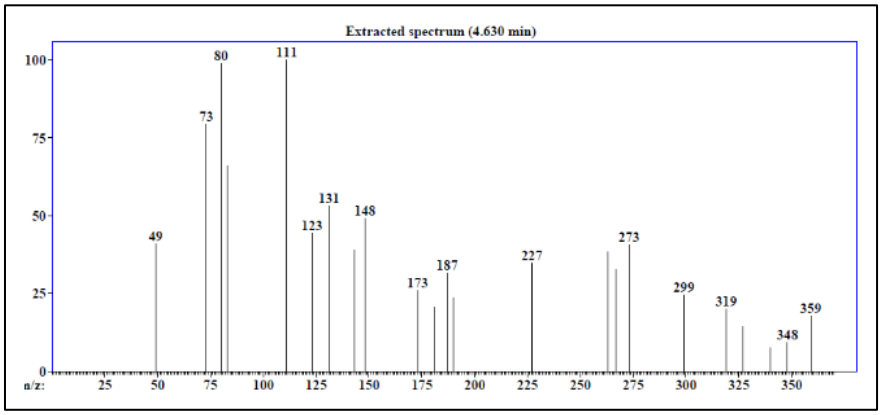

Figure 17 Mass spectrum of the Schiff base ligand [L1]

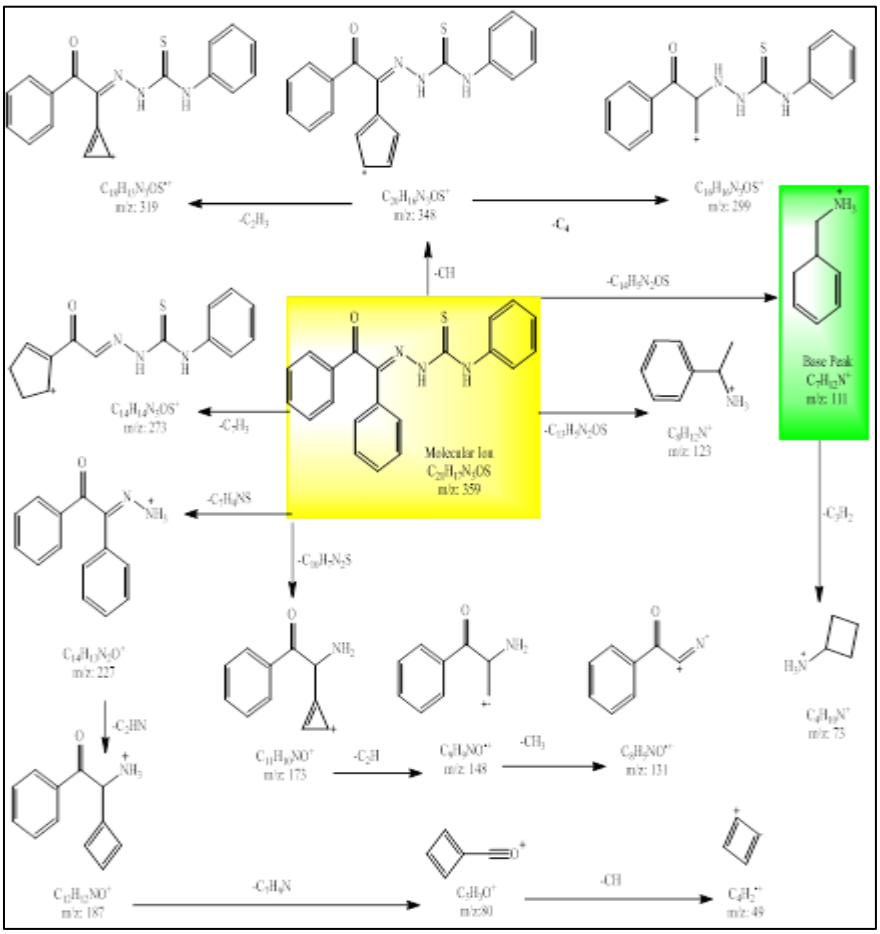

Figure 18 Proposed fragmentation pathway of ligand L1

The mass spectra of [L1] and [L2] each show a molecular ion peak consistent with the calculated molecular weights of 359.4 and 361.4 g/mol, respectively (Table 3), together with fragmentation patterns arising from cleavage of the C=N and C-N/N-N linkages, which is typical of thiosemicarbazone-type Schiff bases and provides further confirmation of the proposed structures [9].

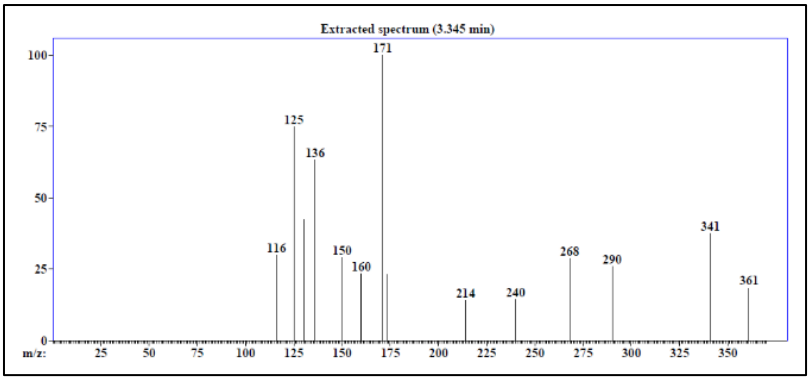

Figure 19 Mass spectrum of the Schiff base ligand [L2]

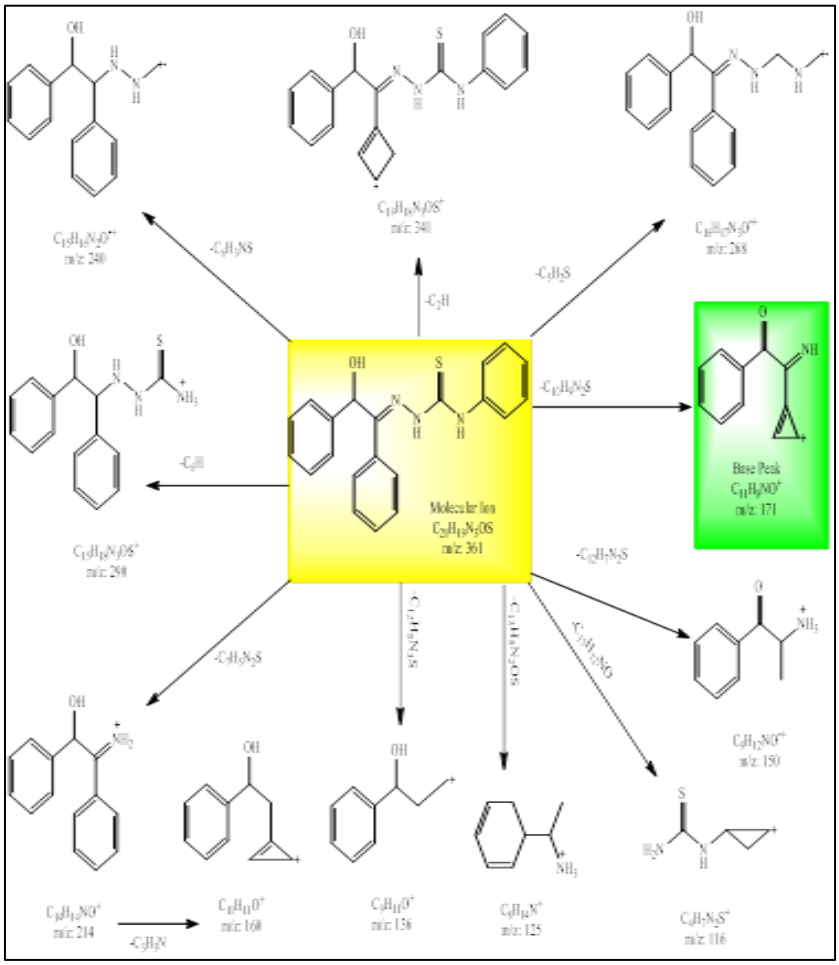

Figure 20 Proposed fragmentation pathway of ligand L2

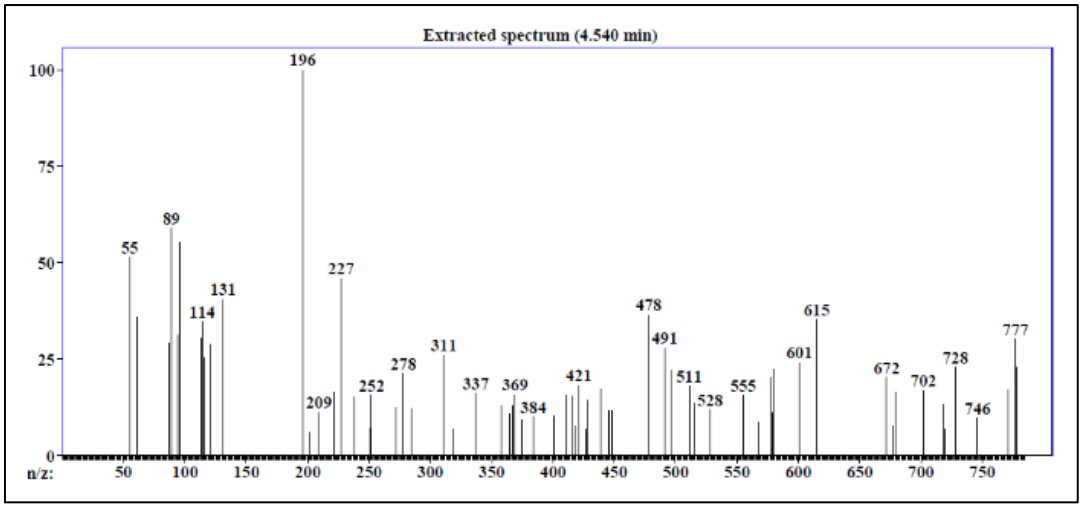

Figure 21 Mass spectrum of the complex [Ni(L1)2]

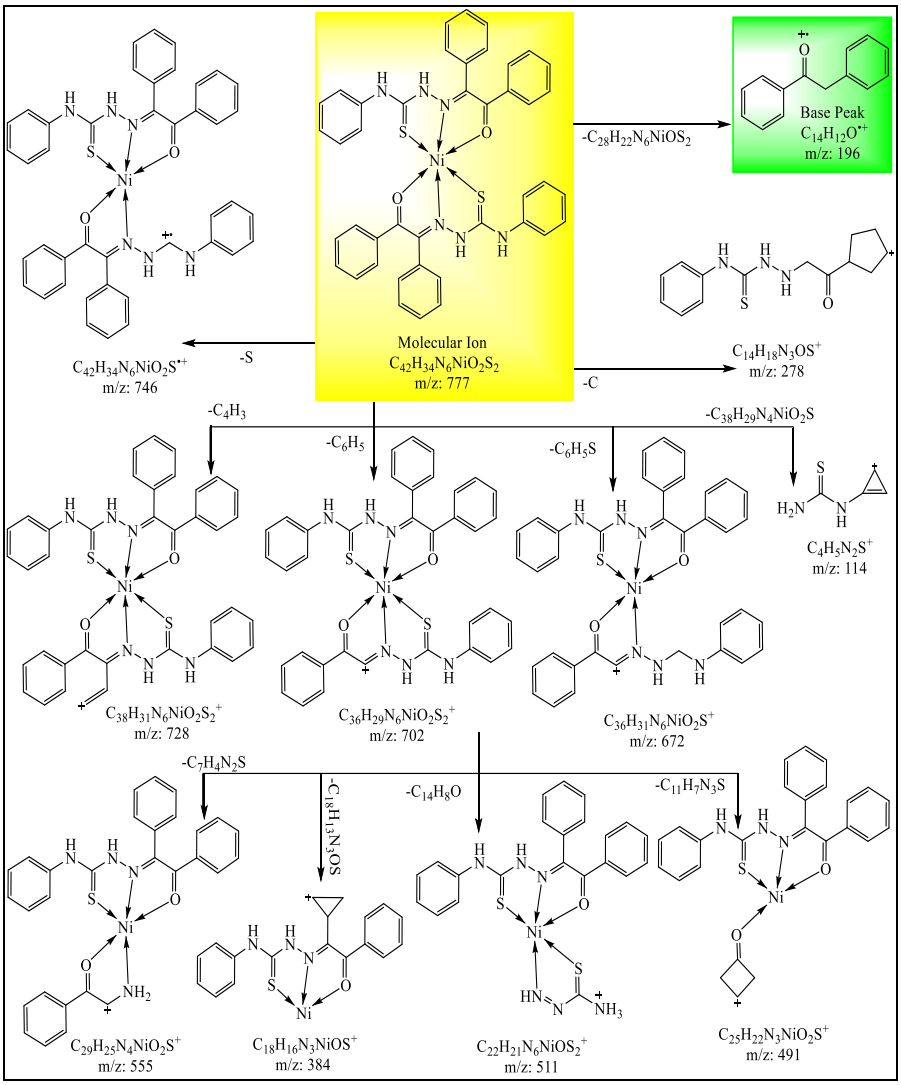

Figure 22 Proposed fragmentation pathway of the complex [Ni(L1)2]

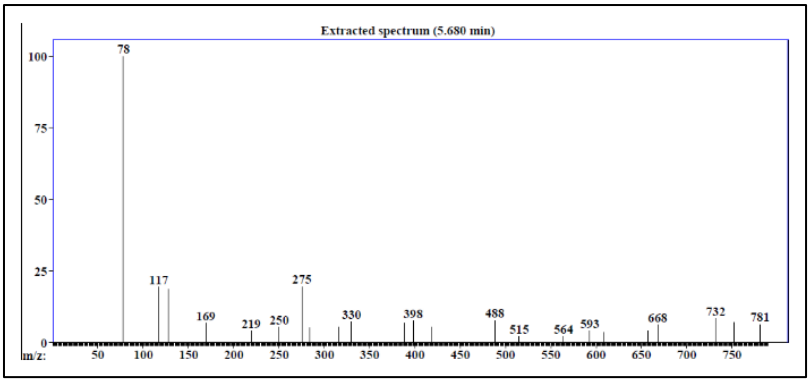

Figure 23 Mass spectrum of the complex [Ni(L2)2]

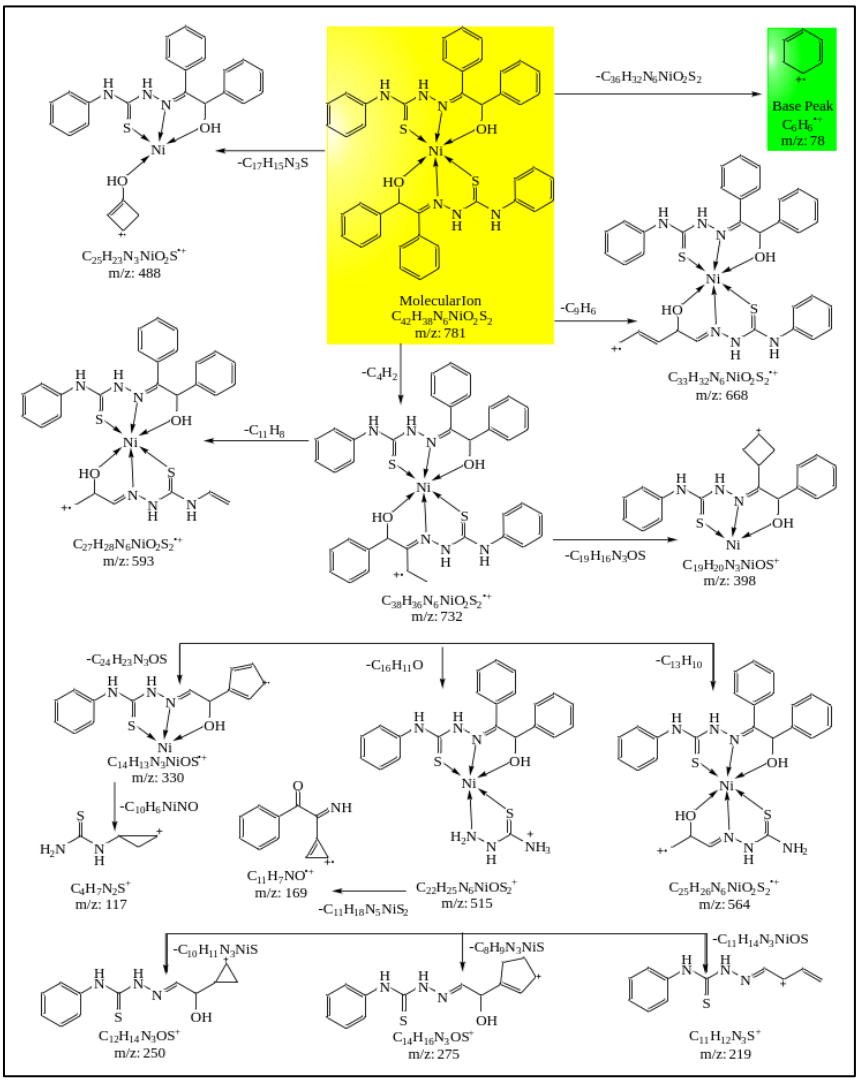

Figure 24 Proposed fragmentation pathway of the complex [Ni(L2)2]

3.6. Magnetic susceptibility and proposed geometry

As expected for closed-shell organic molecules, both free ligands [L1] and [L2] are diamagnetic (μeff = 0 B.M.); upon complexation, the Co(II) and Ni(II) chelates become paramagnetic, and the magnitude of the observed magnetic moment provides a first indication of the coordination geometry adopted by each metal ion [15,17].

The Ni(L1) and Ni(L2) complexes show reduced magnetic moments of 1.41 and 1.30 B.M., respectively, intermediate between the diamagnetic value expected for square-planar low-spin Ni(II) and the higher moments (≈ 2.9–3.4 B.M.) typical of purely octahedral/tetrahedral high-spin Ni(II); such intermediate values are commonly rationalized in terms of a spin equilibrium or a mixture of octahedral and square-planar Ni(II) environments in the solid state [14,15].

The Co(L1) and Co(L2) complexes display magnetic moments of 3.17 and 2.62 B.M., respectively, corresponding to one unpaired electron; such reduced, low-spin-type moments for Co(II) are generally interpreted as arising from a distorted octahedral or square-planar environment with a significant orbital contribution, rather than the free-ion high-spin value expected for regular octahedral Co(II) [11,17].

Table 10 Magnetic moments and proposed geometries of the Co(II) and Ni(II) complexes

Comp.	M.W. (g/mol)	μeff (B.M.)	No. of unpaired e^-	Magnetic behavior	Proposed geometry
L1	359.45	0	0	Diamagnetic	-
L2	361.46	0	0	Diamagnetic	-
[Ni(L1)2]·H2O	781.61	1.41	2 (mixed spin)*	Paramagnetic	Octahedral / Sq. planar
[Ni(L2)2]·H2O	777.59	1.30	2 (mixed spin)*	Paramagnetic	Octahedral / Sq. planar
[Co(L1)2]	777.83	3.17	1 (low spin)	Paramagnetic	Distorted octahedral
[Co(L2)2]	781.86	2.62	1 (low spin)	Paramagnetic	Square planar / Octahedral

3.7. Frontier molecular orbitals (HOMO/LUMO)

The calculated HOMO and LUMO energies of [L2] and its Co(II) and Ni(II) complexes show that the HOMO-LUMO energy gap decreases sharply on complexation, from 1.258 eV for the free ligand to 0.100 eV for [Co(L2)2]·H2O and 0.076 eV for [Ni(L2)2]·H2O, indicating that coordination to the metal center substantially narrows the frontier orbital gap [18,19].

Such a pronounced reduction of the HOMO-LUMO gap upon chelation is generally taken as evidence of enhanced electronic delocalization and softness of the complexes relative to the free ligand, and is consistent with reports that metal coordination of azomethine/thioamide Schiff bases increases chemical reactivity and charge-transfer character, factors that are frequently correlated with the biological/binding potential of such complexes [20,21].

Table 11 HOMO/LUMO energies and energy gap (ΔE) of [L2] and its Co(II)/Ni(II) complexes

#	Compound	HOMO (eV)	LUMO (eV)	ΔE (eV)
1	[L2]	-0.844	+0.414	1.258
2	[Co(L2)2]·H2O	+0.356	+0.456	0.100
3	[Ni(L2)2]·H2O	+0.059	+0.136	0.076

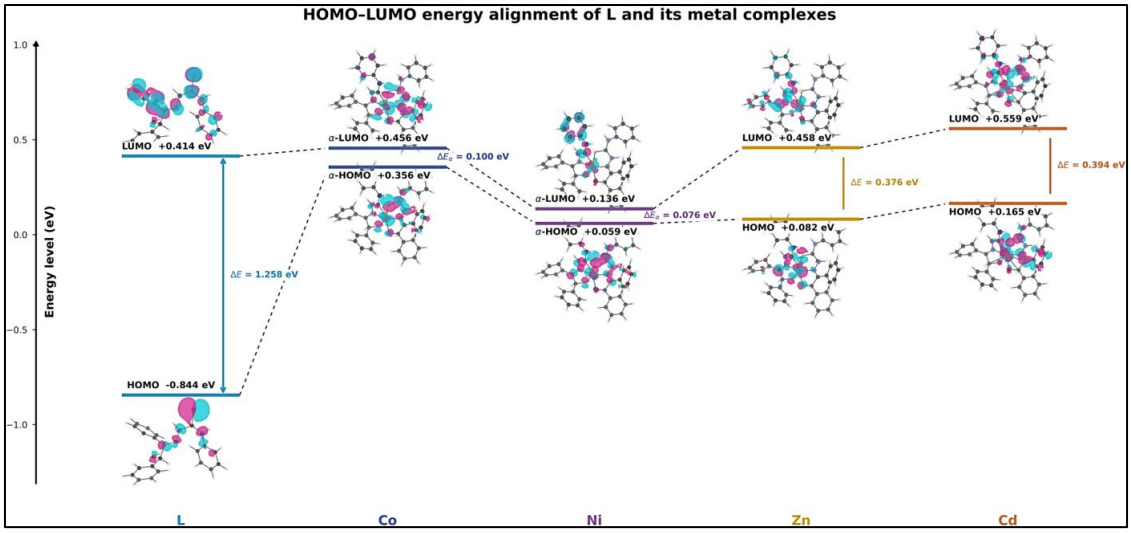

Figure 25 Frontier molecular orbital (HOMO/LUMO) diagrams of [L2] and its Co(II)/Ni(II) complexes

3.8. Thermogravimetric analysis (TGA)

Thermogravimetric analysis of the free ligands and of the hydrated Co(II) and Ni(II) complexes was carried out under a nitrogen atmosphere at a heating rate of 10 °C min^{-1} up to 800 °C; the free ligands show an initial low-temperature mass-loss stage attributable to surface moisture or occluded solvent, followed by successive stages corresponding to loss of lattice/hydrogen-bonded water and progressive decomposition of the organic framework, ultimately leaving a non-volatile carbonaceous/inorganic residue [22,23].

Table 12 Thermal decomposition data of the Schiff base ligand [L1]

Stage	Temp. range (°C)	Mass loss obs. (%)	Mass loss calc. (%)	Assignment
1	18.11–30.34	1.560	–	Surface moisture / adsorbed solvent traces
2	120.84–166.62	10.438	10.02	Loss of 2 H2O (or equivalent occluded solvent)
3	170.81–234.76	29.227	29.24	Loss of a benzoyl (PhCO) fragment
4	304.64–569.51	33.081	33.14	Loss of an oxidized organic (C7H5NO) fragment

Table 13 Thermal decomposition data of the Schiff base ligand [L2]

Stage	Temp. range (°C)	Mass loss obs. (%)	Mass loss calc. (%)	Assignment
1	119.61–179.67	19.334	19.93	Loss of 4 H2O (or equivalent occluded solvent)
2	188.03–245.81	16.859	16.35	Loss of a thiosemicarbazone (HN=C=S) fragment
3	281.54–305.11	13.100	12.73	Loss from the (OH) and (C=N–N) region as (H2O – N2)
4	316.51–368.21	16.375	16.34	Overlapping decomposition of the organic backbone (C2H5NO equivalent)
5	405.84–647.59	7.183	7.48	Loss of HCN or small gases with carbonaceous residue

For [L1], the largest mass-loss stages (Table 12) are attributed to sequential loss of occluded water/solvent, a benzoyl (PhCO) fragment, and an oxidized organic residue, while for [L2] (Table 13) an additional stage corresponding to loss of a thiosemicarbazone (HN=C=S)-type fragment is resolved, consistent with the different substitution pattern of the benzoin-derived ligand; in both cases the observed mass losses agree closely with the calculated values for the proposed fragments, supporting the assigned molecular structures [24,25].

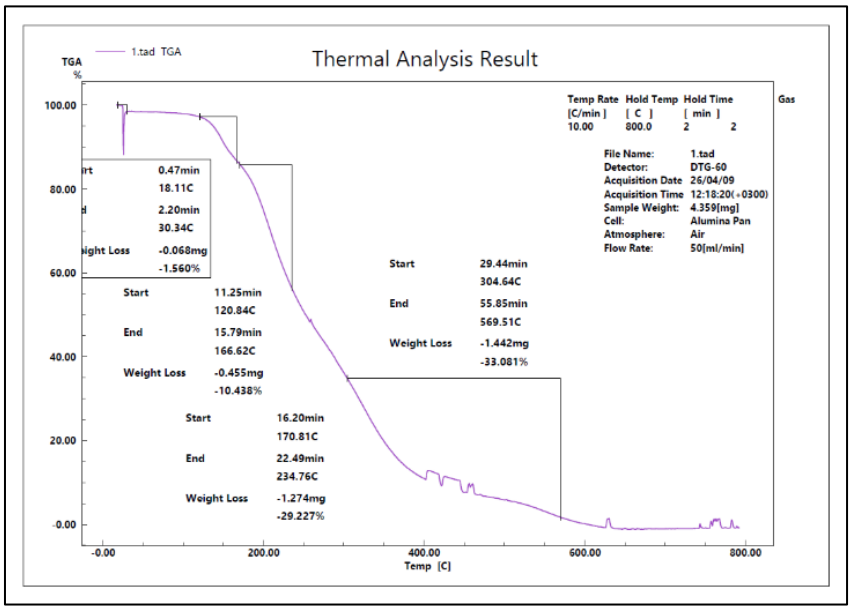

Figure 26 TGA thermogram of the Schiff base ligand [L1]

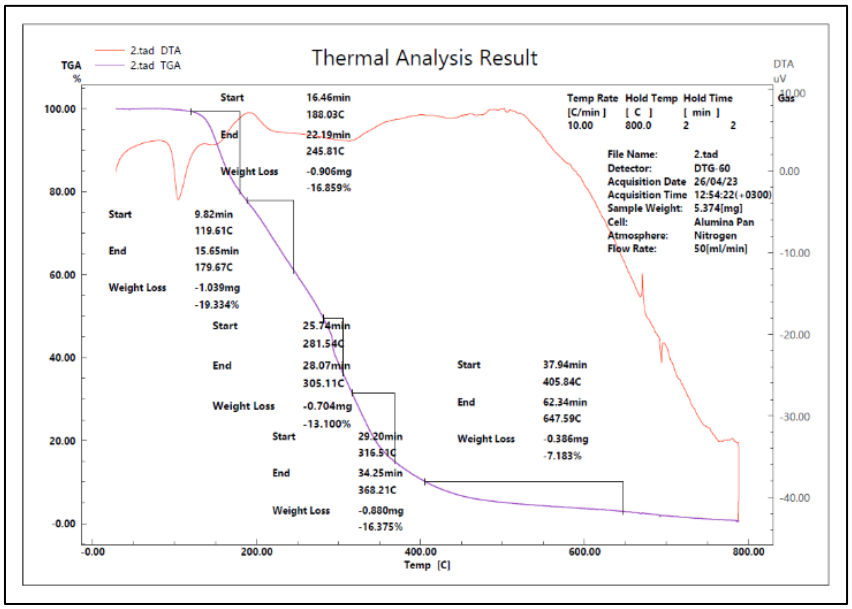

Figure 27 TGA thermogram of the Schiff base ligand [L2]

Thermogravimetric analysis of the complex [Co(L1)2] (proposed formula [Co(C42H34N6O2S2)], M = 781.86 g mol^{-1}) was carried out on a 3.425 mg sample under N2 from room temperature to 800 °C at 10 °C min^{-1}. The complex decomposed in three principal stages: an initial major stage (69.03–277.01 °C, observed loss 2.848 mg, 83.153%) attributed to decomposition of the bulk C37H25N6O2S2 organic fragment (calculated 2.846 mg, 83.107%); a second stage (280.47–404.15 °C, observed 0.278 mg, 8.117%) attributed to loss of a residual C5H3 carbonaceous/aromatic fragment (calculated 0.276 mg, 8.068%); and a third stage (404.49–668.79 °C, observed 0.225 mg, 6.569%) attributed to decomposition of a further C4H3 residue (calculated 0.224 mg, 6.532%), leaving a final non-volatile, cobalt- and

carbon-rich residue of 0.074 mg (2.161% of the initial mass) that cannot be assigned an exact chemical identity from the TGA curve alone [22,25].

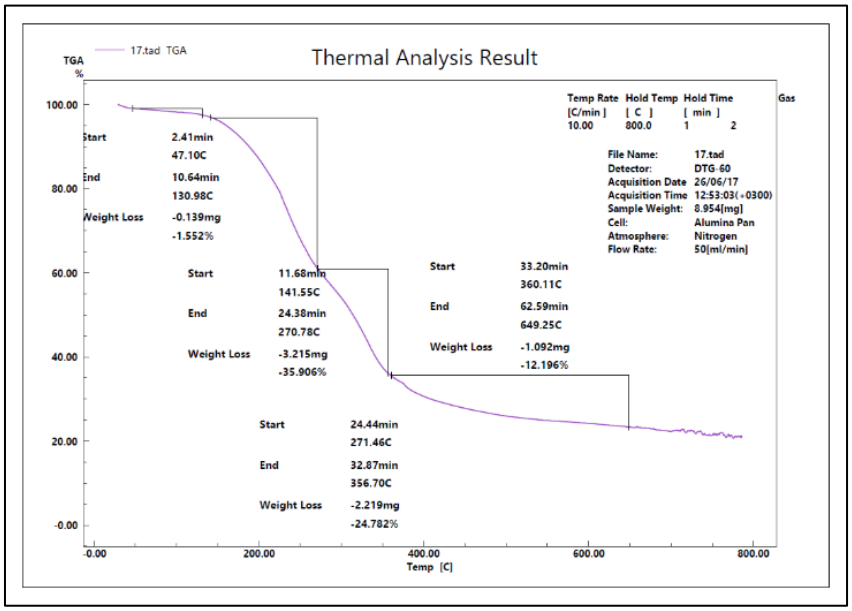

Figure 28 TGA thermogram of the complex [Co(L1)2]

An analogous three-stage decomposition profile was obtained for [Co(L2)2] (proposed formula [CoC42H38N6O2S2], M = 781.86 g mol^{-1}; initial sample mass 3.425 mg, N2 atmosphere, 10 °C min^{-1} to 800 °C): the first and dominant stage (69.03–277.01 °C) corresponded to decomposition of the bulk organic ligand framework (observed 2.848 mg, 83.153%; calculated for C37H25N6O2S2, 2.846 mg, 83.107%); the second stage (280.47–404.15 °C) corresponded to loss of a residual C5H3 fragment (observed 0.278 mg, 8.117%; calculated 0.276 mg, 8.068%); and the third stage (404.49–668.79 °C) corresponded to decomposition of a C4H3 residue (observed 0.225 mg, 6.569%; calculated 0.224 mg, 6.532%). The final residue reached 0.074 mg (2.161%), giving a total observed mass loss of 97.839% against a calculated total of 97.707% — a close agreement that supports the proposed molecular formula of the complex; since the analysis was performed under an inert N2 atmosphere, the successive stages reflect pyrolytic decomposition and gradual carbonization rather than complete oxidative combustion, and the fragment assignments should be regarded as consistent with the observed mass losses rather than as direct proof of the volatile decomposition products[23,25].

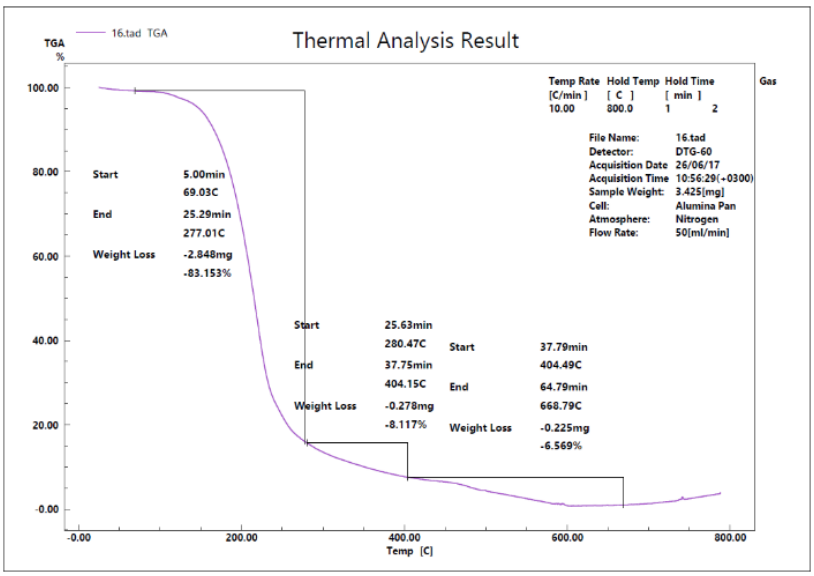

Figure 29 TGA thermogram of the complex [Co(L2)2]

3.9. Molecular docking with Phosphodiesterase 3A (PDE3A)

Phosphodiesterase 3A (PDE3A) was selected as the target enzyme for the in silico docking evaluation of [L1] and [L2] because of its established role in cyclic-nucleotide signaling and its reported relevance as both a therapeutic target and a biomarker in cardiovascular and oncological contexts, including gastrointestinal stromal tumors and other PDE3A/SLFN12-expressing malignancies [26,27].

Docking of [L1] and [L2] into the PDE3A active site was carried out following standard protocols in which the ligand poses are ranked by docking score and evaluated for hydrogen-bond donor/acceptor interactions and interatomic distances with active-site residues, an approach widely used to rationalize the substrate-competitive binding mode of PDE3-family inhibitors [8,28].

Both ligands formed multiple hydrogen-bond interactions (donor and acceptor type) with PDE3A active-site residues at interaction distances in the 2.8–4.3 Å range, with [L1] and [L2] achieving comparable docking scores of −6.30 and −6.32 kcal/mol and RMSD values of 1.58 and 1.67 Å, respectively, indicating stable and comparable predicted binding modes for the two ligands within the enzyme active site [5].

Table 14 Molecular docking parameters of [L1] and [L2] with PDE3A

Compound	E (kcal/mol)	Distance (Å)	Interaction	RMSD	Docking Score
[L1]	-2.4 / -6.9 / -1.1 / -0.8 / -2.4	2.84 / 2.97 / 4.19 / 4.29 / 4.14	H-donor / H-donor / H-acceptor / H-acceptor / H-acceptor	1.5812	-6.3010
[L2]	-5.9 / -1.5 / -0.9 / -2.4 / -1.0	2.92 / 3.89 / 4.02 / 3.79 / 3.00	H-donor / H-acceptor / H-acceptor / H-acceptor / H-acceptor	1.6716	-6.3170

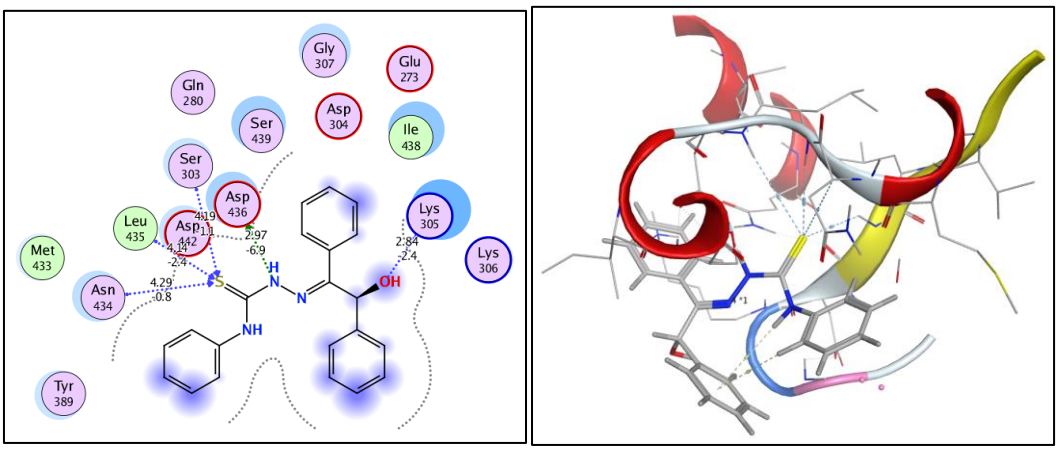

Figure 30 Molecular docking pose of ligand [L1] within the PDE3A active site

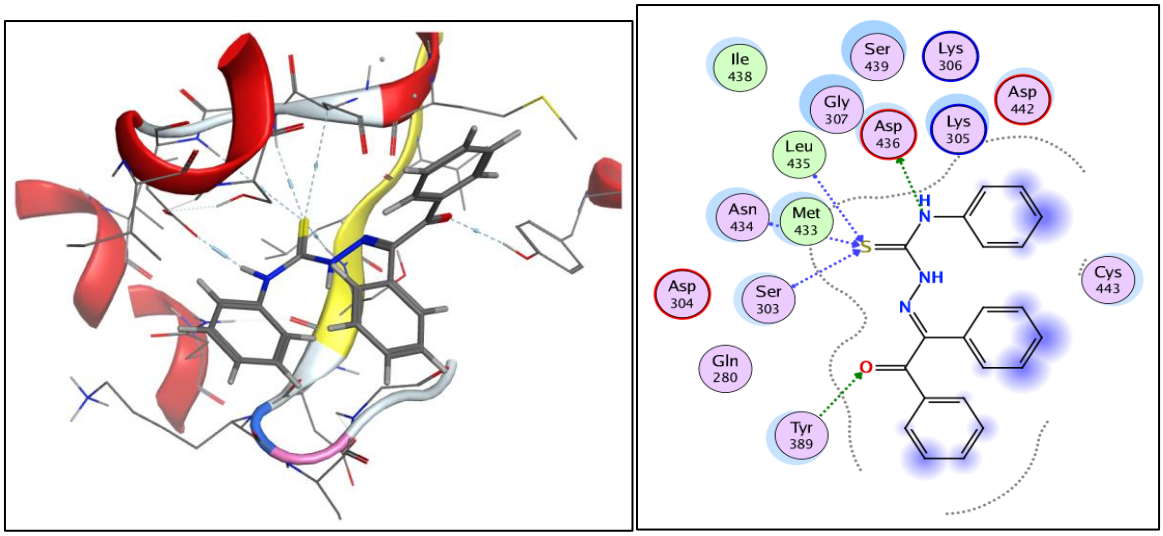

Figure 31 Molecular docking pose of ligand [L2] within the PDE3A active site

These docking results suggest that both thiosemicarbazone-derived Schiff base ligands can be accommodated within the PDE3A active site through a network of hydrogen bonds comparable in strength and distance to those reported for other Schiff base and pyridazinone/pyrazolone-type PDE3A-interacting scaffolds, supporting their consideration as candidate leads for further, experimentally validated PDE3A-directed biological evaluation[7,29].

4. Conclusion

Two thiosemicarbazone-based Schiff base ligands, [L1] and [L2], were synthesized in good purity from benzil and benzoin, respectively, and characterized together with their Co(II) and Ni(II) complexes by FT-IR, UV-Vis, 1H-/13C-NMR, mass spectrometry, magnetic susceptibility, thermogravimetric analysis and HOMO/LUMO calculations. The combined spectral, electronic and magnetic data support coordination through the azomethine nitrogen and thioamide sulfur/nitrogen donors, and the diagnostic LMCT and spin-allowed d-d transitions (^{4}T1g(F)→^{4}A2g(F)/^{4}T1g(P) for the Co(II) complexes and ^{3}A2g(F)→^{3}T1g(d-d) for the Ni(II) complexes) provide direct electronic-spectral evidence for octahedral geometry at both metal centers in all four hydrated chelates. Complexation was found to markedly narrow the HOMO-LUMO energy gap relative to the free ligand, consistent with enhanced electronic reactivity upon chelation, while stage-resolved TGA data for the ligands and their Co(II) complexes showed good agreement between observed and calculated mass losses, supporting the proposed molecular formulae and decomposition pathways. Molecular docking of both ligands against PDE3A revealed comparable, favorable binding scores and multiple hydrogen-bonding interactions with the enzyme active site, indicating that this class of thiosemicarbazone Schiff base ligands merits further biological investigation as potential PDE3A-interacting scaffolds.

Compliance with ethical standards

Disclosure of conflict of interest

No conflict of interest to be disclosed.

References

[1] Kumar, A. et al. Synthesis and structural characterization of mixed ligand metal complexes from terephthalaldehyde bis(thiosemicarbazone) and alanine. Results in Chemistry, 2024. https://doi.org/10.1016/j.rechem.2024.101316

[2] Thiosemicarbazides, 1,3,4-thiadiazole Schiff base derivatives of transition metal complexes as antimicrobial agents. ResearchGate, 2023. https://www.researchgate.net/publication/376458813

[3] Abou Melha, K. S. et al. Spectral, Molecular Modeling, and Biological Activity Studies on New Schiff's Base of Acenaphthaquinone Transition Metal Complexes. Bioinorganic Chemistry and Applications, 2021. https://doi.org/10.1155/2021/6674394

[4] Meena, R. et al. Schiff bases and their metal complexes: Synthesis, structural characteristics and applications. In Schiff Base in Organic, Inorganic and Physical Chemistry, IntechOpen, 2023. https://www.intechopen.com/chapters/89503

[5] A novel pyridine-based Schiff base with multi-target pharmacological potential: synthesis, biological evaluation and molecular docking analysis. Turkish Journal of Analytical Chemistry, 2026. https://dergipark.org.tr/en/pub/turkjac/article/1872743

[6] Kelly, M. P. et al. Therapeutic targeting of 3',5'-cyclic nucleotide phosphodiesterases: inhibition and beyond. Nature Reviews Drug Discovery, 2019. https://www.nature.com/articles/s41573-019-0033-4

[7] Beyond the heart - Exploring the therapeutic potential of PDE3 inhibitors. Journal of Research in Pharmacy, 2025. https://dergipark.org.tr/en/pub/jrespharm/article/1684882

[8] Docking and quantitative structure-activity relationship of bi-cyclic heteroaromatic pyridazinone and pyrazolone derivatives as PDE3A inhibitors. PLoS ONE / PMC, 2017. https://pmc.ncbi.nlm.nih.gov/articles/PMC5720733/

[9] Synthesis, Spectral Characterization, and Antimicrobial Activity of Two Novel Schiff Bases Derived from Thiosemicarbazide and Mononuclear 3d Transition Metal Complexes. Oriental Journal of Chemistry, 2023. https://www.orientjchem.org/vol38no6/

[10] Spectroscopic, Thermal, and Antimicrobial Studies of Co(II), Ni(II), Cu(II), and Zn(II) Complexes Derived from Bidentate N,S Ligands. PMC, 2012. https://www.ncbi.nlm.nih.gov/pmc/articles/PMC3512225/

[11] Bioactive Co(II), Ni(II), and Cu(II) Complexes Containing a Tridentate Sulfathiazole-Based (ONN) Schiff Base. Molecules/PMC, 2021. https://www.ncbi.nlm.nih.gov/pmc/articles/PMC8161335/

[12] Núñez-Montenegro, A. et al. New thiosemicarbazone Schiff base ligands: synthesis, characterization, catecholase study and hemolytic activity. Journal of Inorganic Biochemistry, 2019. https://www.sciencedirect.com/science/article/abs/pii/S0022286019316758

[13] Synthesis and structural studies of complexes of Co(II), Ni(II) and Cu(II). Journal of Chemical Sciences. https://www.ias.ac.in/article/fulltext/jcsc/100/05/0363-0373

[14] Impact of tetrahedral and square planar geometry of Ni(II) complexes with (pseudo)halide ligands on magnetic properties. Inorganica Chimica Acta, 2018. https://www.sciencedirect.com/science/article/abs/pii/S0020169318308752

[15] Preparation and Characterization of Nickel and Cobalt Complexes (magnetic moment/geometry relationships). https://frankwalmsley.com/nickel_cobalt_experiment_2010.pdf

[16] Venkatesh, G. et al. Synthesis and Spectroscopic Characterization of Schiff Base Metal Complexes, Biological Activity, and Molecular Docking Studies. ACS Omega, 2024. https://pubs.acs.org/doi/10.1021/acsomega.3c08526

[17] Anomalous Magnetic Moment (Inorganic Chemistry-II, Metal-Ligand Bonding). e-PG Pathshala. https://epgp.inflibnet.ac.in/epgpdata/uploads/epgp_content/chemistry/07.inorganic_chemistry-ii/33._anomalous_magnetic_moment/et/8821_et_et.pdf

[18] Design and Bio Evaluation of Schiff Base and Their Metal Complexes: A Green Route to Potential Anticancer Agents. PMC/ACS Omega, 2025. https://pmc.ncbi.nlm.nih.gov/articles/PMC12947217/

[19] Metal complexes featuring a quinazoline Schiff base ligand and glycine: synthesis, characterization, DFT and molecular docking analyses. BMC Chemistry, 2024. https://link.springer.com/article/10.1186/s13065-024-01239-7

[20] Synthesis, characterization, DFT calculation, and biological activity of a new Schiff base ligand and its ZnO and Co3O4 nano-metal oxide complexes. BMC Chemistry, 2025. https://link.springer.com/article/10.1186/s13065-025-01673-1

[21] Exploring the chemical and biological landscape of a Nickel(II) Schiff base complex via azomethine linkage. Scientific Reports, 2025. https://www.nature.com/articles/s41598-025-31991-2

[22] Synthesis, characterization, DFT calculations and biological activity of new Schiff base complexes. Heliyon, 2023. https://pmc.ncbi.nlm.nih.gov/articles/PMC10447992/

[23] Synthesis, characterization and thermogravimetric analysis of Co(II), Ni(II), Cu(II) and Zn(II) complexes supported by an ONNO tetradentate Schiff base. Arabian Journal of Chemistry, 2015. https://www.sciencedirect.com/science/article/pii/S1319610315000071

[24] Metal complexes derived from tetradentate Schiff base ligands: synthesis, spectroscopic analysis, thermogravimetric degradation and antimicrobial activities. Journal of Molecular Structure, 2023. https://www.sciencedirect.com/science/article/abs/pii/S0022286023012498

[25] Thermal Analysis of Copper Metal Complexes: Insights from TGA and DSC. Oriental Journal of Chemistry, 2026. https://www.orientjchem.org/vol41no4/

[26] Nazir, M. et al. Targeting tumor cells based on Phosphodiesterase 3A expression. Experimental Cell Research, 2017. https://www.sciencedirect.com/science/article/abs/pii/S0014482717305803

[27] Phosphodiesterase 3A: a new player in development of interstitial cells of Cajal and a prospective target in gastrointestinal stromal tumors (GIST). PMC, 2017. https://www.ncbi.nlm.nih.gov/pmc/articles/PMC5522287/

[28] Molecular docking of competitive phosphodiesterase inhibitors. PubMed, 2001. https://www.ncbi.nlm.nih.gov/pubmed/11752202

[29] An, R. et al. PDE3A inhibitor anagrelide activates death signaling pathway genes and synergizes with cell death-inducing cytokines to selectively inhibit cancer cell growth. PMC, 2019. https://pmc.ncbi.nlm.nih.gov/articles/PMC6780660/